Landslides (2019) 16:1425–1435
DOI 10.1007/s10346-019-01190-y
Received: 29 January 2019
Accepted: 25 April 2019
Published online: 11 May 2019

Tommaso Carlà · Teresa Nolesini · Lorenzo Solari · Carlo Rivolta · Luca Dei Cas · Nicola Casagli

Rockfall forecasting and risk management along a major transportation corridor in the Alps through ground-based radar interferometry

Abstract Rockfalls are a recurrent cause of disruption for transportation corridors running along the bottom of U-shaped alpine valleys. In some scenarios, risk may effectively be reduced only by implementing an early-warning system able to give notice of incipient failures on the slope. This paper describes a successful example of rockfall forecasting and risk management in proximity of the Gallivaggio sanctuary (San Giacomo Valley, Central Italian Alps). Since 2016, a Ground-Based Synthetic Aperture Radar continuously monitored a roughly 500-m high, sub-vertical granitic slope. Monitoring data evidenced the presence and continued movement of a ~ 5000 m^3 highly unstable mass, having a projected fall trajectory directly threatening the sanctuary and the adjacent segment of a national road. Traffic and access to the sanctuary were regulated by a sequence of alert thresholds, and restrictive orders were issued according to the activity of the instability. The rock mass eventually fell, and the failure-time was accurately predicted several hours in advance. Despite damage to both the road and buildings, the timely evacuation of the area prevented any loss of life. The case study provides a reference framework to better manage rockfall risk in areas where the installation of adequate protective barriers is not technically feasible.

Keywords Rockfall · GBInSAR · Early-warning · Tertiary creep · Failure-time prediction

Introduction

Transportation corridors cutting through alpine terrain are critically exposed to rockfalls. These instabilities can occur in response to different mechanisms and driving forces, and with a frequency that is highly variable depending on environmental conditions and lithostructural predisposition (Hungr et al. 2014). The quantitative estimation and baseline monitoring of rockfall hazard along transportation corridors is an increasingly important topic of research, due to the great impact on the travelling public and on local populated areas (Lato et al. 2009; Salvini et al. 2013; Macciotta et al. 2015; Kromer et al. 2017). Defining expected trajectories, return periods, and failure locations is of primary importance to support decision making and design appropriate remediation measures (Hungr et al. 1999; Macciotta et al. 2016). However, this is sometimes not sufficient for reducing risk to tolerable levels in scenarios characterized by a diffuse and persistent human presence, owing to the uncertainties inherent to probabilistic analyses and to the rapid nature of failure development. In this sense, an effective strategy consists of the implementation of an early-warning system supported by a near-real-time slope monitoring network (Intrieri et al. 2012). Response actions aimed at preserving safety can be undertaken once preselected thresholds of alarm are exceeded (Crosta and Agliardi 2003; Loew et al. 2017).

Challenges related to the monitoring of high-mountain rock walls are significant, often resulting in undersampled or poorly collected data. Difficult site accessibility and incomplete understanding of potential rockfall source areas are the most prominent factors constraining the applicability of conventional instruments (e.g., crackmeters, extensometers, and survey prisms). In general, point-wise information are not able to capture the amount and complexity of ongoing instabilities at the scale of an entire slope. Furthermore, previously stable slope sectors may be abruptly remobilized as the rock mass loses strength through degradation and disturbance effects. Remotely acquired high-resolution imaging data (e.g., lidar and photogrammetry) may be used to detect failure precursors during the damage accumulation phase of the rock surface (Lato et al. 2015; Sättele et al. 2016; Kromer et al. 2017), but they are not a viable option for early-warning purposes if hourly or sub-hourly monitoring is required. This gap has been filled by the Ground-Based Interferometric Synthetic Aperture Radar (GBInSAR) technique, which combines sub-millimetric displacement measurement accuracy, wide area coverage, high spatial resolution, and high frequency of data acquisition and processing (Casagli et al. 2010; Farina et al. 2013; Monserrat et al. 2014; Atzeni et al. 2015).

This paper describes a successful example of rockfall forecasting and risk management supported by GBInSAR monitoring in proximity of the Gallivaggio sanctuary (San Giacomo Valley, Central Italian Alps). The sanctuary is located at the foot of a roughly 500-m high, sub-vertical granitic slope (Fig. 1). It is also adjacent to the National Road (NR) 36, which climbs up to the Splügen Pass at the border between Italy and Switzerland. Monitoring of the slope started in 2011 in the form of discontinuous GBInSAR campaigns; in 2016, the device was installed permanently with the aim of giving notice of any incipient failure.

The early-warning system was stress-tested when a ~ 5000 m^3 markedly disintegrated rock mass at the top of the rock wall became evidently unstable. Travelling along the NR 36, as well as the access to the sanctuary, were consequently regulated by a sequence of alert thresholds representative of increasing risk scenarios. Each risk scenario was associated with specific procedures of traffic management and/or evacuation. The GBInSAR captured a gradual rise in deformation rate of this mass, likely anticipating an evolution towards failure. Alert thresholds were occasionally exceeded, prompting the respective response actions. The instability experienced a final acceleration from the morning of 29 May 2018, and the failure-time (4:32 p.m. local time on 29 May 2018) was accurately predicted several hours in advance. Thanks to the previously issued restrictive orders, no injuries or fatalities were counted.

The case study demonstrates how GBInSAR monitoring can serve as a decisive tool for mitigating rockfall risk. The proposed

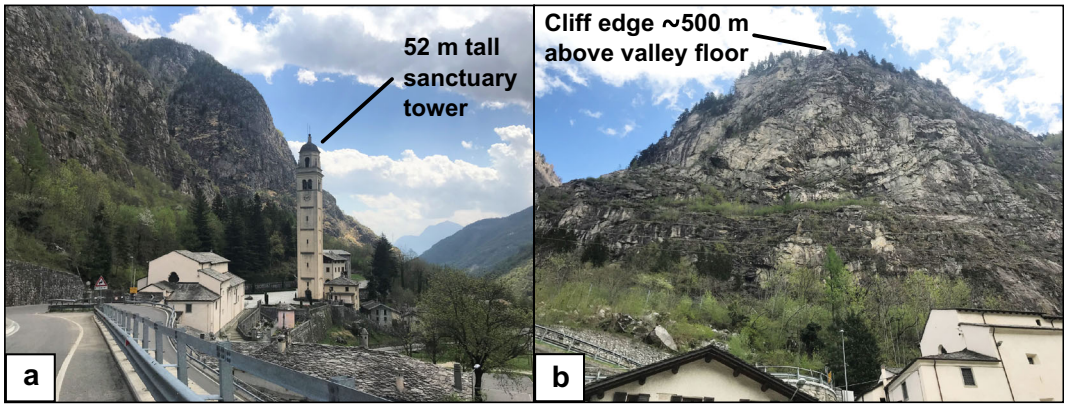

Fig. 1 **a** View of the Gallivaggio sanctuary from the NR 36 and **b** of the overhanging granitic slope

framework is intended for scenarios where the safety of people cannot be guaranteed by physical barriers or other retaining structures, but only by delineating emergency protocols and by communicating evacuation orders.

Study area

Elements at risk

The Italian NR 36 provides the main access to the Chiavenna Valley (north of Lake Como, Italy) and to the Swiss canton of Grisons. It begins in the city of Milan and culminates at over 2000 m a.s.l. at the Splügen Pass, which marks the border between Italy and Switzerland. In its last stretch, the roadway sweeps through the floor of the San Giacomo Valley (the northern branch of the Chiavenna Valley) with a quick succession of sharp hairpin bends, wedged between towering rock walls and the left (east) bank of the Liro Creek (Fig. 2). Traffic is concentrated during summer and winter, the peak seasons for tourism. It is estimated that, on average, between 150,000 and 200,000 tourists travel to the region every year.

Situated along the initial section of the mountain road, the Gallivaggio sanctuary is a renowned pilgrimage destination and an important cultural heritage site, with many pieces of fine art (some of which date back to the seventeenth century) therein preserved. The building complex lies between km 126 of the NR 36 and a roughly 500 m high, sub-vertical granitic slope (Fig. 1). It is therefore extremely vulnerable to rockfalls, as the narrow and steep configuration of the valley makes the installation of active protective barriers of adequate height or capacity not feasible from a technical point of view. Passive defense systems between the sanctuary and the rock wall comprise a 150-m long, 4.5–9-m high protection embankment; a 3.5-m high catch fence on top of the embankment; and a 10-m wide catch ditch between the slope and the embankment (Figs. 2 and 3). Still, rockfalls of various sizes have repeatedly reached, and caused minor damages to both the NR 36 and the sanctuary in the recent past. Blocks may in fact unpredictably bounce and fragment over the slope, producing trajectories that easily fly over the catch fence. This possibility is greatly enhanced when large failure volumes are involved.

Temporary road closures have severe socioeconomic repercussions on the municipalities at higher elevation, that are thereby subject to losing the sole transportation corridor connecting them with the rest of the country. As the topmost segment of the Splügen Pass is blocked by snow during the winter, several villages and hamlets (for a total of almost 1500 permanent residents), plus a number of popular ski resorts and other tourist facilities, may suffer complete isolation for prolonged periods of time. In this eventuality, people may travel to the lower end of the San Giacomo Valley only by walking a mountain trail on the west side of the Liro Creek.

Geological and geomorphological setting

The N-S trending San Giacomo Valley belongs to the upper Penninic Zone and represents the natural divide between the Lepontine and Rhaetian Alps. The regional geological setting is dominated by the emplacement of sub-horizontal gneissic bodies (Tambò and Suretta units), each composed of a polycyclic and polymetamorphic basement of paragneiss with thin intercalations of amphibolite and orthogneiss (Ferrari et al. 2014). The Tambò nappe forms a 3.5 to 4 km thick crystalline sliver unconformably overlain by a Mesozoic metasedimentary cover unit (Schmid et al. 1990; Baudin et al. 1993). The study area is found in the southern part of the Tambò nappe, featuring a late Variscan intrusive complex named Truzzo granite (Figs. 2 and 3). The structure of the Truzzo granite transitions from that of a mesoscopic undeformed granite to that of a highly strained orthogneiss (Marquer et al. 1994).

The geomorphology widely reflects the erosive action of a Late Würm glacier, which filled the San Giacomo Valley over a thickness of several hundreds of meters and modeled it to its current U-shape between 20,000 and 10,000 ka. Shallow and deep-seated failures are favored by the combination of high-relief landscape, lithostructural controls, environmental factors (e.g., precipitation, thermal stresses, freeze-thaw cycles), and paraglacial stress release (Cossart et al. 2008). Four joint sets determine the basis for the formulation of prisms and tetrahedrons, which may give place to planar or wedge mechanisms once the necessary kinematic requirements are fulfilled. The state of the Truzzo granite at the surface is locally disrupted and shattered down to a depth of a few meters, further facilitating the development of joint persistence (average joint spacing of approximately 0.5 m) and the production of isolated blocks, which typically range between 0.1–

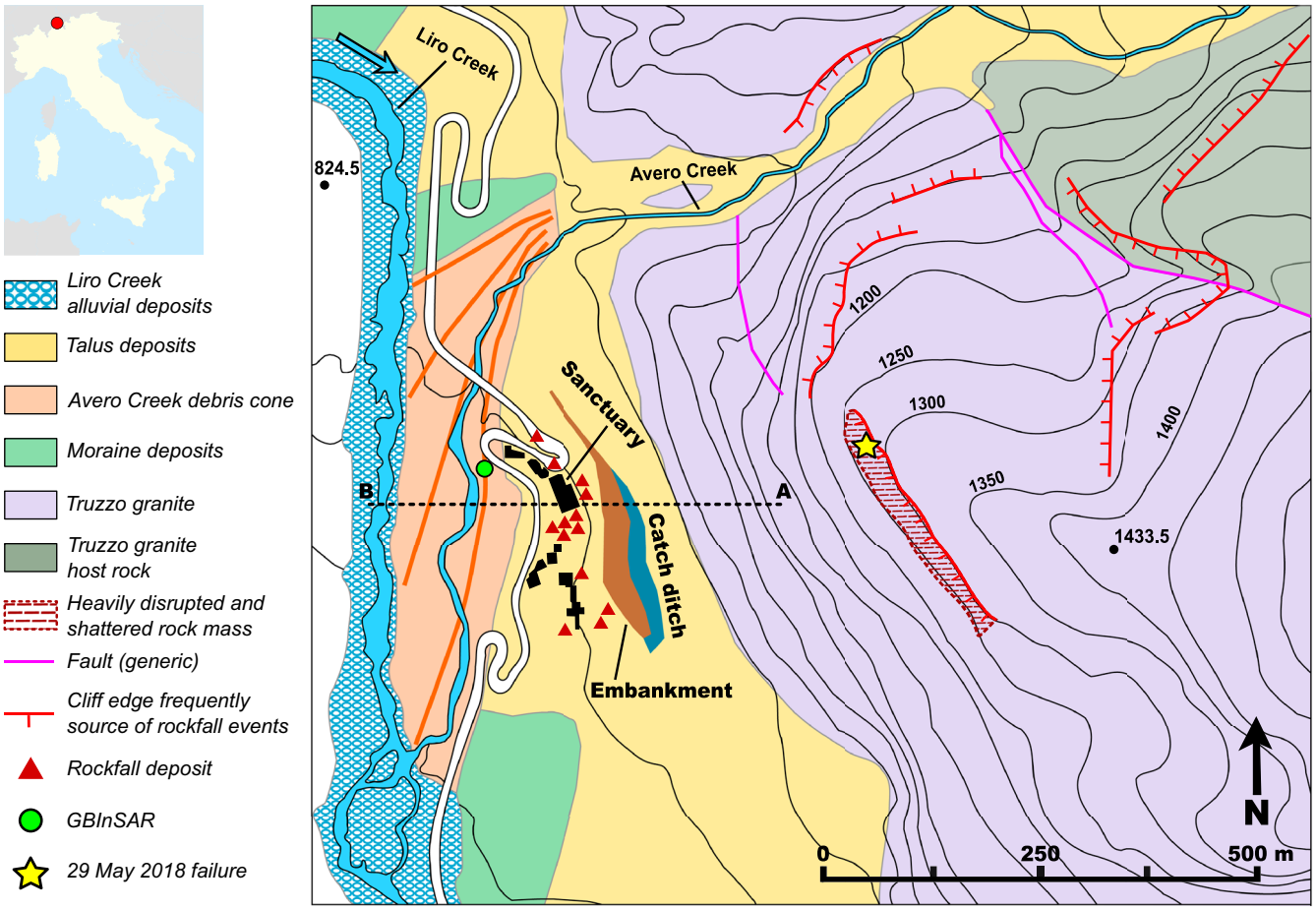

Fig. 2 Geological map of the study area. The red hatching marks the sector of the rock wall from which most of the rockfall events that affected the sanctuary or the adjacent structures (see rockfall deposits) presumably originated. Some of these blocks can still be observed in the field today

2 m^3 in size. In the study area, these effects are especially pronounced in the higher portions of the slope, where a more pervasive rock foliation (or "orthogneissic facies") is observed and the fracture planes are more exposed to weathering.

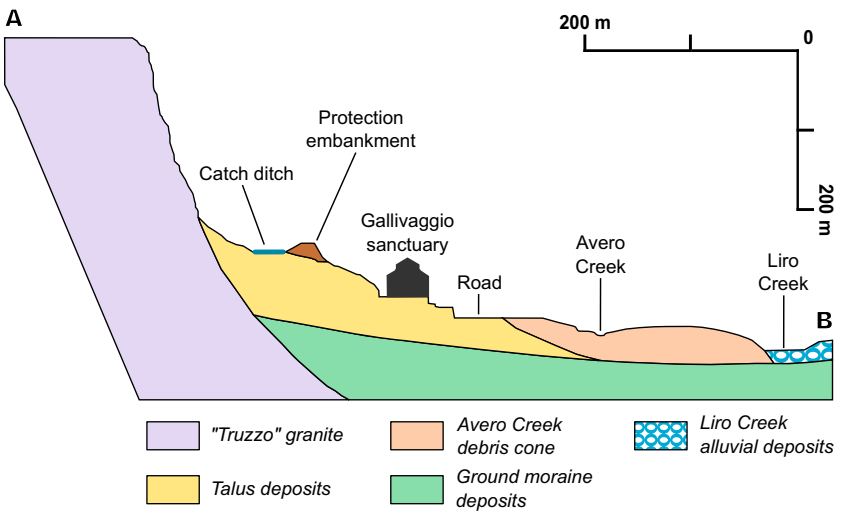

Fig. 3 Schematic cross-section along the AB trace in Fig. 2

Description of the ~ 5000 m³ instability

The 29 May 2018 failure originated at the top of the rock wall looming over the Gallivaggio sanctuary. Before the event, the instability appeared as a markedly disintegrated rock mass with very weak internal structure, lacking base support, and jutting out of the slope (Fig. 4a). Such an indentation could have derived from the previous detachment of other blocks, which left the overlying mass in precarious equilibrium. The size of the 29 May 2018 failure was 20–25 m in height, 21 m in width, and 8–11 m in thickness, yielding an estimated volume of ~ 5000 m³. The path of the projected fall trajectory directly threatened the NR 36 and the sanctuary.

The geometry of the failure block was defined by a compound sliding plane. In particular, the main morphological features included (Fig. 4b) the following:

- a sub-vertical joint as rear release surface, penetrating at least 20 m into the slope and opening up to as much as 2 m in width;
- a steeply dipping (55–60°) joint acting as basal release surface, over which the sliding movement predominantly occurred;
- at the top of the mass, a chaotic pile of blocks and crushed debris indicating significant lowering of the ground surface.

Slab-shaped fragments were also deposited right at the foot of the instability, having fallen from the rock face above. This could be the consequence of tensile failure of the highly fractured rock mass, and possibly of the accumulation of strain energy ensuing from the shear stresses acting on the basal sliding plane (Rosser et al. 2007; Kilburn 2012). The source areas of at least two minor rockfalls (volume of few m³) that reached the valley floor on 7 June 2017 and 13 April 2018 (prior to the main failure in May 2018) were indeed located along the perimeter of the instability. This is in agreement with the notion that increasing breakdown rates of the slope surface via rockfall is a key precursor to larger failures (Rosser et al. 2007; Stock et al. 2012; Royán et al. 2015).

Slope monitoring and early-warning system

In 2016, after several discontinuous campaigns carried out in the previous years, a GBInSAR was permanently deployed on the left bank of the Liro Creek (Fig. 2) to monitor the deformation of the overhanging slope in near-real-time. Permanent monitoring was initiated once sufficient economic sources for sustaining a year-round service became available. The discontinuous campaigns confirmed that slow creep movements were present at high elevations on the slope, coherently with the spatial distribution of the weaker facies of the Truzzo granite (see "Geological and geomorphological background"); the lower sectors appeared essentially stable.

The GBInSAR operates in Ku-band (~ 17 GHz) and moves along a mechanical linear rail to create a synthetic aperture. Distance (range) and direction (azimuth) of the targets (i.e., pixels) are attained through transmission and reception of the electromagnetic wave. In principle, line-of-sight (LOS) displacements of each pixel are calculated with sub-millimetric accuracy by exploiting the phase difference of the back-scattered signal between two or more coherent acquisitions, and by assessing the contribution that actually stems from the ground movement (Leva et al. 2003; Luzi et al. 2006; Casagli et al. 2010; Atzeni et al. 2015). As the availability of large sets of images (equivalent to some days of acquisition) enables the application of averaging and ad hoc statistical tools, the technique is scarcely affected by atmospheric noise and has proved to be suitable for analyzing the evolution of mass movements in high alpine terrain (Noferini et al. 2007; Barla et al. 2010; Del Ventisette et al. 2012; Kieffer et al. 2016; Barla et al. 2017). No artificial reflectors on the slope are

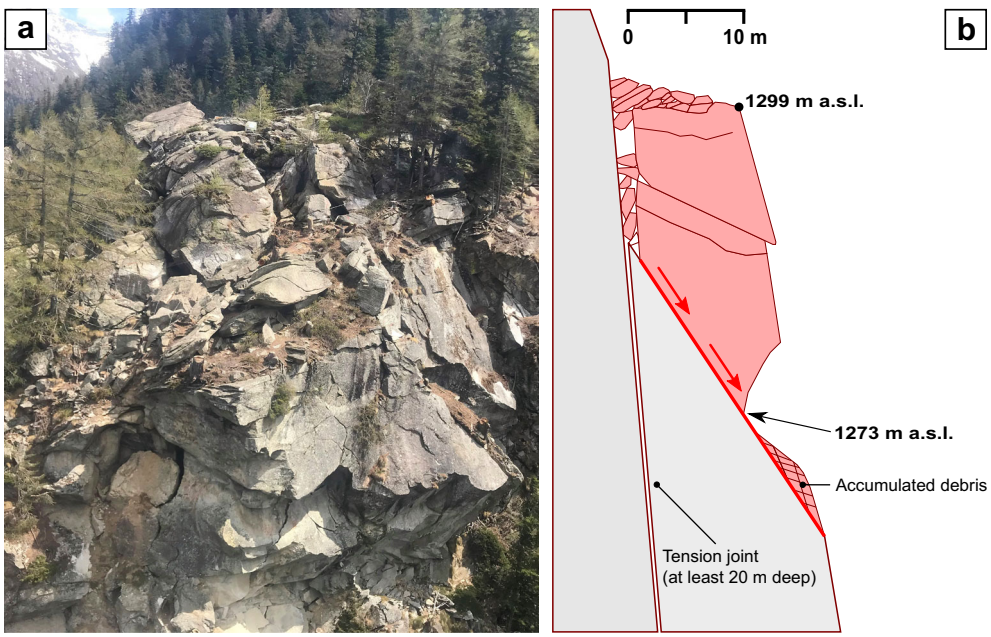

Fig. 4 **a** Frontal view and **b** cross-sectional sketch of the ~ 5000 m³ instability prior to the 29 May 2018 failure

required, assuming that some parts of the area of interest are stable and exploitable for minimizing atmospheric contributions.

In the employed configuration, range and azimuth resolution of the pixels covering the topmost portion of the rock wall were approximately 75 cm and 180 cm, respectively. Even though precursors to small rockfalls may not be detected because of insufficient pixel resolution, the primary focus was the timely identification of larger rockfalls that could not be contained by the existing protective barriers. While an exact estimation of the minimum detectable rock volume across the entire slope is difficult, some authors have made use of GBInSAR monitoring for predicting failures from few 10^2 m^3 down to few 10^1 m^3 (Mazzanti et al. 2015; Kieffer et al. 2016; Carlà et al. 2017; Mononen et al. 2018). Given the favorable LOS, and the short distance between the instrument and the foot of the slope (~ 150 m), it was anticipated that the minimum detectable rock volume would be within the range of values reported in the above-cited literature.

Depending on the magnitude and trend of the deformation rates, the frequency of image acquisition could be as low as 2 min, so as to avoid phase wrapping issues. These arise when movements during an acquisition step are larger than half a wavelength (~ 8.8 mm), and appears in the interferogram as a homogeneous pattern of phase cycles (i.e., interferometric fringes) over the rapidly deforming area (Casagli et al. 2010). A shorter acquisition step will therefore diminish the likelihood of phase ambiguity, at the cost of increased storage capacity needed for the greater number of images acquired.

A sequence of thresholds representative of increasing risk scenarios was established as the central component of the early-warning system. The thresholds were defined by an amount of displacement over unit of time, with displacements being tracked for each pixel of the deformation map. Acceleration was not regarded as a reference parameter, since it is more prone to noise-induced variability and thus to generating false alarms. Each risk scenario was initially associated with different levels of surveillance activity; in the aftermath of the reactivation of the ~ 5000 m^3 instability in April 2018 (see next section), specific procedures of traffic management and/or evacuation were also introduced. No rockfall event had been monitored in the study area prior to this study; therefore, the behavior of the rock mass prior to a failure was not known with certainty. As a result, the thresholds and the levels of alarm (Table 1) were based on similar experiences portrayed in the literature (e.g., Loew et al. 2017) and on the following considerations:

- the relatively small size of the kinematically feasible phenomena could imply very rapid processes of failure development, allowing for little forewarning;
- the foregoing could be exacerbated by the intrinsically brittle behavior of crystalline rock types (Rose and Hungr 2007);
- abrupt changes in environmental conditions (e.g., strong rainfalls or thermal excursions) could have a more severe and nearly instantaneous effect on heavily broken rock masses;
- a conservative approach was preferred due to the entity of the risk posed to public safety, hence the small gaps between the different threshold values.

The 29 May 2018 failure

Radar data and sequence of events

During the first years of monitoring, the ~ 5000 m^3 instability showed a steady-state creep, with average velocities of 1.5–2 cm/year. At the end of 2017 and in the following months, these slowly increased to values of 3–5 cm/year, only to experience an additional and sudden increase in April 2018; no significant movements were observed in other parts of the slope (Fig. 5). The GBInSAR data highlighted a 30 × 35 m deforming sector, slightly larger than the size of the eventual failure block. Much of this supplementary deformation was concentrated below the lower boundary of the instability, and could be attributed to mechanisms of damage propagation and to the incremental opening of the rear tension joint at greater depth (Fig. 3).

Within the deforming sector (Fig. 5), ten highly coherent pixels were selected as surface control points indicative of the evolution of the instability. Each control point was uniquely identified by a time series of displacement, automatically updated on a regular basis just minutes after each new image acquisition.

Figure 6 depicts the full time series of displacement between 1 June 2017 and 4:15 pm (local time) on 29 May 2018. As previously mentioned, a slight, gradual increase of yearly velocities began in the late summer of 2017. Afterwards, the instability experienced a sudden acceleration on 13 April 2018 (peak velocities of 5–10 mm/day), together with the occurrence of a minor rockfall that originated from the same area. Some tiny fragments, ranging from 10^{-1}–10^{-2} m^3 in size and accounting for a total rock volume of few m^3, reached the NR 36 and the sanctuary. The events prompted the activation of the ultimate code of alarm (very high = red color; Table 1) and the immediate introduction of procedures regulating traffic and access to the site. Velocities fluctuated around the 4 mm/day threshold until the end of the month, before decreasing temporarily to 1–2 mm/day.

The nature of the acceleration, the notable rates at which the slope kept deforming, as well as the occurrence of the minor rockfall itself, were all elements suggesting that the instability was now in an incipient state of failure, where equilibrium was vastly achieved through simple frictional resistance with negligible contribution of internal rock strength. This reflects the culmination of the progressive failure process: the excess of shear stress induces micro-cracks coalescence and the consecutive rupture of intact rock bridges along the sliding plane until the latter extends to the point that kinematic release becomes possible (Eberhardt et al. 1998). Accordingly, it was decided to reduce the early-warning system to only the two uppermost levels of alarm—that is, a "high" alarm (Table 1) was maintained also when velocities occasionally dropped below the 3 mm/day threshold. Whenever the "very high" alarm was not in place, the continuous monitoring of the slope allowed authorities to open the NR 36 during fixed daily time frames—5 to 8 a.m., 12 to 2 p.m., and 6 to 9 p.m. In one of such circumstances, with velocities having temporarily settled around values of 1 mm/day, the pieces of fine art preserved in the sanctuary were relocated.

Finally, displacements started to escalate on the evening of 28 May 2018. The next morning, about 9 h before ultimate failure, the monitoring system captured the onset of a slope acceleration in

Table 1 Early-warning system for the management of rockfall risk in the area of the Gallivaggio sanctuary. The procedures of traffic management and/or evacuation introduced in April 2018 are provided in italics

Level of alarm	Threshold	Response actions
Moderate	1.5 mm/day or 3 mm over 72 hours	▪ Increased surveillance activity on site ▪ Acquisition of measurements at manually-surveyed fixed monuments using a portable distometer, as ground check of the GBInSAR data ▪ *Possible introduction of traffic restrictions along the NR 36*
High	3 mm/day	▪ Constant surveillance activity on site ▪ Operations control room manned 24/7 ▪ *Evacuation of the sanctuary* ▪ *Opening of the NR 36 to private vehicles restricted to fixed daily time frames*
Very high	4 mm/day	▪ Constant surveillance activity on site ▪ Operations control room manned 24/7 ▪ *Evacuation of the sanctuary* ▪ *Total closure of the NR 36*

remarkable agreement with a classic tertiary creep curve (Fig. 6). Deformation rates widely exceeded the peak values ever detected up to that moment, climbing to 73.5 mm/h in the case of Point_07. At 1 p.m., the image acquisition frequency was shortened from 14 to 9 min as the phase of the moving pixels approached a full cycle, and then from 9 to 4 min at 3 p.m. After 4:15 p.m., despite the GBInSAR having been pushed to its 2-min limit of image acquisition frequency at 3:45 p.m., measured displacements were no longer reliable because of phase wrapping issues—i.e., the displacements were sufficiently large to justify multiple phase interpretations. Nonetheless, the appearance of at least two interferometric fringes between 4:15 p.m. and 4:32 p.m. verified the persistence of the acceleration, and therefore the imminence of the failure (Fig. 7). The interferogram acquired between 4:32 p.m. and 4:34.p.m. ultimately revealed a complete loss of coherence, consistently with the detachment of material from the slope.

The falling mass crumbled in a myriad of smaller blocks and fragments, forming a huge cloud of dust and debris which ran over the valley floor (Fig. 8a). As expected, a major percentage of the debris inundated violently the area of the Gallivaggio sanctuary and the adjacent segment of the NR 36. The high degree of fragmentation, partially produced through bouncing and partially inherent to the already disintegrated state of the rock mass, meant that the infrastructure did not suffer from irreparable damages. A photo of the rockfall scar is shown in Fig. 8b.

Prediction of the failure

In proximity of the event, the early-warning activities were explicated through the continuous calibration of failure-time predictions with every displacement measurement update. Many approaches rely on the concept that slope velocity increases asymptotically towards infinite prior to failure, a phenomenon

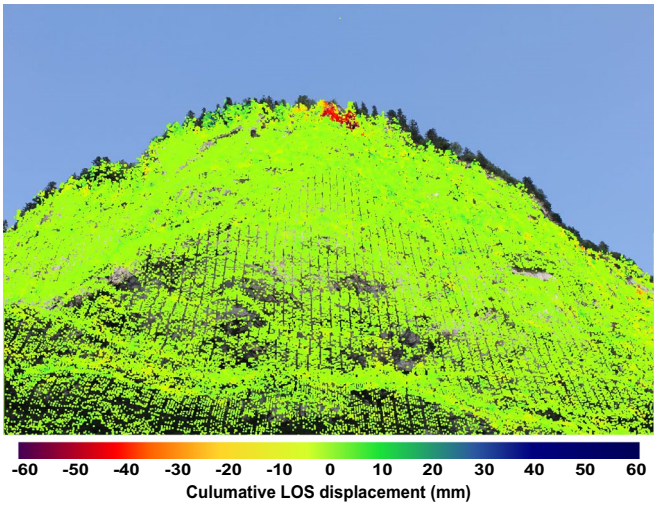

Fig. 5 Map of cumulative LOS displacements measured by the GBInSAR in the period 13–26 April 2018, superimposed on an optical image taken from the look perspective of the instrument. Gray areas over the slope correspond to the parts of the optical image (i.e., rock surface) with no return signal

known as tertiary or accelerating creep (Voight 1989; Crosta and Agliardi 2003; Federico et al. 2012). Contrarily to large-scale failures, this precursor has often a very short duration in small-scale failures in tension or shear involving hard rock masses (Rose and Hungr 2007). Inappropriate sampling rates may thus return seemingly instantaneous displacements that are not meaningful to perform reliable predictions. Given its characteristics (e.g., high sampling rate and high spatial resolution at short baseline distances), the GBInSAR technique is a very efficient way of dealing with this problem (Mazzanti et al. 2015; Carlà et al. 2017).

Tertiary creep stages are usually analyzed graphically by means of the inverse velocity method, according to which the failure-time corresponds to the point of intersection on the abscissa of the extrapolated trend in a plot of 1/velocity versus time (Fukuzono 1985; Voight 1989; Cornelius and Scott 1993; Petley et al. 2002). Figure 9 shows the inverse velocity measurements for three control points of the ~ 5000 m^3 instability above the Gallivaggio sanctuary, based on a 5-point moving average of the data. The onset of the final downward trend can be discerned at about 7:30 a.m. on 29 May 2018 (9 h before the failure). The plot converged decisively after 10:30 a.m. (6 h before the failure): from that moment, all subsequent points were observed to be closely aligned with a definite linear trend. The predicted failure-time was consistently calculated in the interval 4:25–4:45 p.m. For instance, the last prediction for Point_08 (made before the appearance of ambiguities in the interferometric phase, Fig. 7) yielded an expected failure at 4:28 p.m., basically matching the actual failure-time (4:32 p.m.).

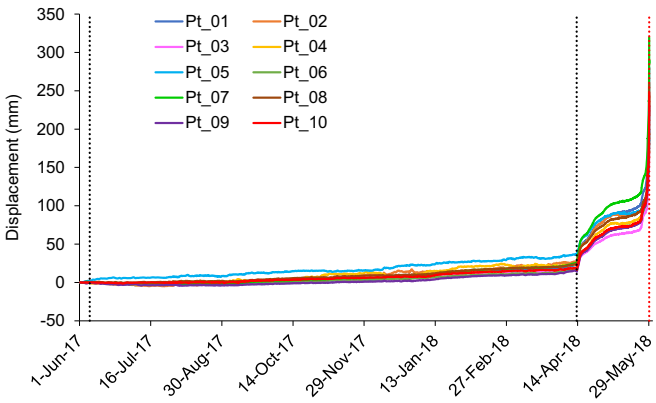

Fig. 6 Displacement time series of the control points between 1 June 2017 and 4:15 p.m. (local time) on 29 May 2018. The black dotted lines point out the 7 June 2017 and 13 April 2018 minor rockfalls, the red dotted line the time of the final failure

Predictions were also performed by means of Hao's method, who recently deduced a new failure-time criterion from a number of laboratory creep experiments on granites (Hao et al. 2016, 2017). The failure-time is determined by the intersection with the time axis of the projected curve of v/a, where v is velocity and a is acceleration. The alleged advantage of this method, which has never been tested on data from actual failures in natural slopes, is that the trend to failure is always linear, whereas it has been demonstrated that the shape of inverse velocity plots could display some variation (Voight 1989; Cornelius and Scott 1993; Petley et al. 2002; Kilburn 2012). On the other hand, the use of the second derivative of the displacement means that data noise will inevitably increase, and smoothing over a wider time window is needed. The v/a versus time measurements for three control points prior to the 29 May 2018 failure, based on a 20-point moving average of the data, are highlighted in Fig. 10. Definite plot convergence was obtained from 3:30 p.m. (1 h before the failure), and again calculated failure-times basically matched the actual failure-time. For instance, the last prediction for Point_01 (made before the appearance of ambiguities in the interferometric phase, Fig. 7) yielded an expected failure at 4:41 p.m.

Lastly, the data analysis was focused on evaluating peak velocity and peak acceleration of the instability as the tertiary creep stage progressed. The idea was first introduced by Federico et al. (2012), who noticed a broadly linear correlation between the logarithm of these parameters near failure for a large number of case studies. The work was later expanded by Carlà et al. (2017), who reviewed GBInSAR data from nine open-pit mine instabilities in hard intrusive rocks; the database was composed of five failures and four "non-failures" (i.e., instabilities undergoing episodes of intense acceleration that eventually did not evolve to failure). The authors found that peak velocity and peak acceleration were linearly correlated in non-logarithmic form too, and were noticeably larger in the five failures. The relative graph, modified with the addition of the case study presented in this paper, is reported in Fig. 11. Prior to the 29 May 2018 failure above the Gallivaggio sanctuary, a peak velocity of 73.5 mm/h and a peak acceleration of 50.6 mm/h^2 were registered at 4:15 p.m. by Point_07, well in line with the previous findings. It should be noted that the aforementioned values constitute a lower-bound estimate, since they refer to LOS measurements. Moreover, larger values would also be derived through phase unwrapping of the data between 4:15 p.m. and 4:32 p.m. (Fig. 7). The results hence corroborated the expectations about the imminence of the failure.

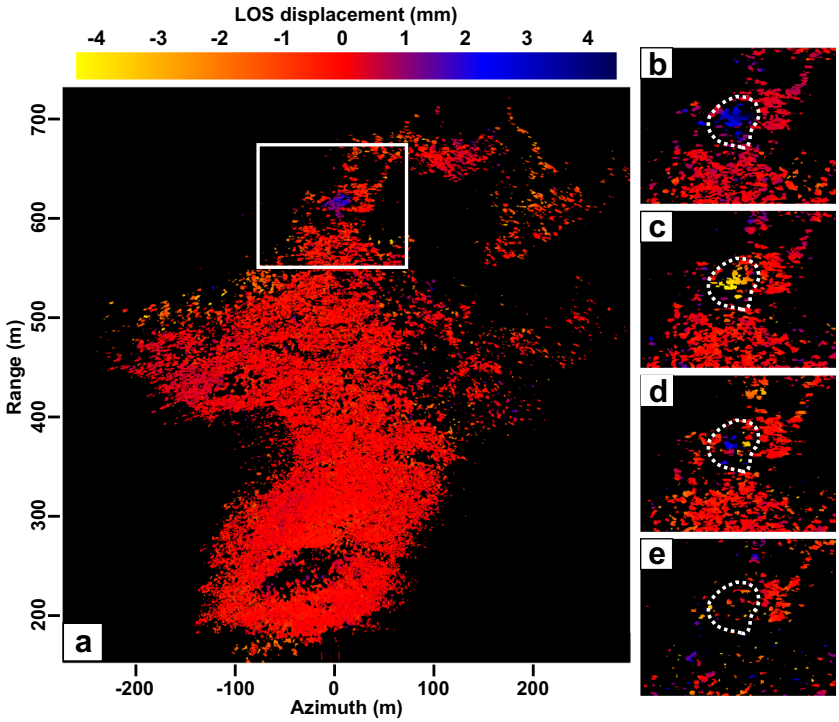

Fig. 7 Two-minute interferograms between 4:08 p.m. and 4:34 p.m. (local time) on 29 May 2018. The white rectangle in (**a**) delimits the area magnified in (**b**–**e**); the dotted polygons in (**b**–**e**) delimit the area of interest. In detail: **a** 4:08–4:10 p.m.: no wrapped phase; **b** 4:10–4:12 p.m.: increase of displacement, no wrapped phase; **c** 4:18–4:20 p.m.: wrapped phase (one fringe); **d** 4:25–4:27 p.m.: wrapped phase (two fringes); **e** 4:32–4:34 p.m.: failure, with general loss of coherence due to detachment of material and formation of a cloud of dust overshadowing the slope. Range and azimuth are the sensor-to-target distance and the direction parallel to the synthetic aperture, respectively

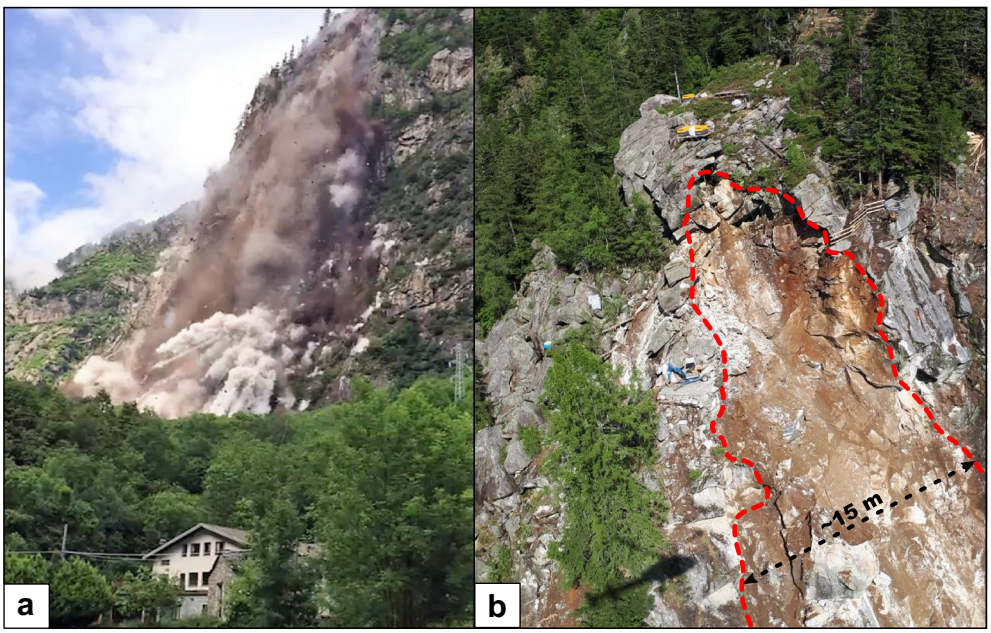

Fig. 8 **a** 29 May 2018 failure and **b** scar left on the rock wall. Infrastructure and equipment in (**b**) were deployed before the failure by the technical staff in charge of the surveillance and ground check activities

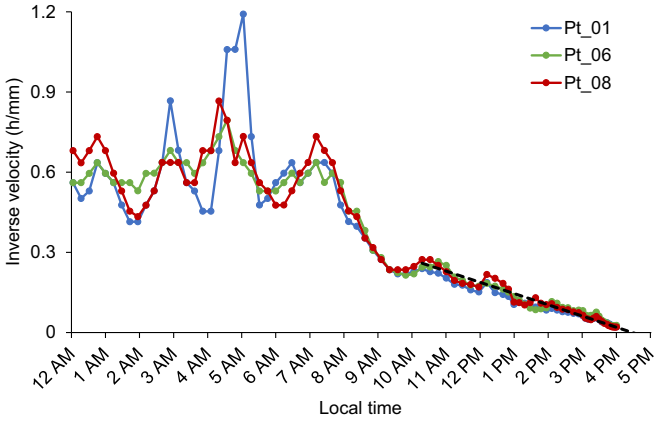

Fig. 9 Failure-time prediction of the 29 May 2018 failure by means of the inverse velocity method. The measurements affected by wrapped phase (Fig. 7c–e) are not included. The three control points in the figure were picked for illustrative purposes

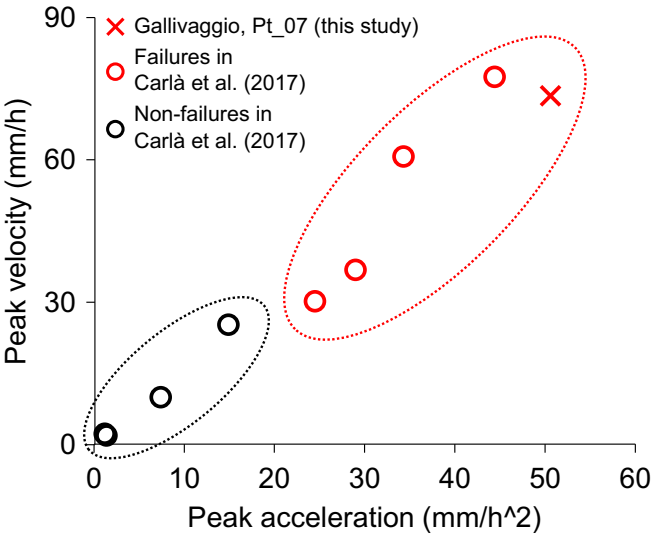

Fig. 11 Graph of peak velocity versus peak acceleration, modified after Carlà et al. (2017)

Discussion and conclusions

The 29 May 2018 failure above the Gallivaggio sanctuary testifies the tremendous impact that even rockfalls of relatively small size can have on communities and infrastructures in alpine terrain. The event was hardly out of the ordinary for the area; the San Giacomo Valley has a history of countless failures, some of which have been far larger in size. Unfavorable combinations of fall trajectory and height, kinetic energy of the blocks, and location of the exposed elements are sufficient to produce extraordinary levels of risk without necessarily implying exceptional volumes of rock.

Near real-time slope monitoring is still rarely used for rockfall forecasting and risk management. Typical solutions either focus on rockfall magnitude–frequency relationships and probabilistic analyses of risk distribution, or on the detection of pre-failure damage features (e.g., deformation, tension crack opening, precursory rockfalls) through baseline monitoring techniques (Hungr et al. 1999; Rosser et al. 2007; Stock et al. 2012; Macciotta et al. 2015, 2016; Kromer et al. 2017). However, these are not suited to the implementation of an early-warning system, which in some scenarios may be the only viable option for reducing risk to tolerable levels. Other approaches propose to provide early-warning by linking the likelihood of rockfall to precipitation, freeze-thaw cycles, or other external triggers (Chau et al. 2003; Krautblatter and Moser 2009; Mateos et al. 2012). While noteworthy statistical correlations may be found, some problems remain. The influence of environmental conditions is in fact not univocal: it is dependent on rock strength, degree of damage accumulation, joint structure, overall quality of the rock mass, and local factors. Once a critical threshold of damage within the rock is reached, the formation of macro-scale release surfaces is primarily governed by internal mechanisms, and secondarily by external triggers (Eberhardt et al. 1998). It follows that a single instability may, for example, react very differently to precipitation events of comparable intensity occurring at different times.

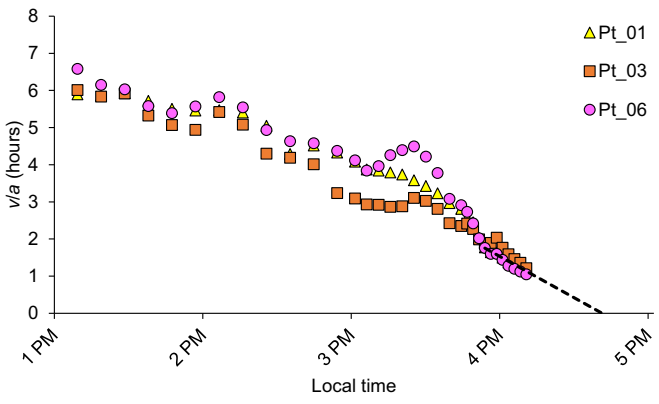

Fig. 10 Failure-time prediction of the 29 May 2018 failure by means of Hao's method. The measurements affected by wrapped phase (Fig. 7) are not included. The three control points in the figure were picked for illustrative purposes

Figure 12 shows the graph of maximum hourly rainfall intensity (measured on a daily basis) versus cumulative displacement from January to May 2018. Rainfall data were collected by a pluviometer installed in the lower San Giacomo Valley at an elevation of 1060 m a.s.l. The onset of the final acceleration was concurrent with the strongest rainfall since the beginning of the year. On the other hand, rainstorms during the previous summer season repeatedly generated rainfall intensities about two to three times the value of 9.6 mm/h registered on 27 May 2018, with no response of the instability being caused whatsoever. This could have been misleading if rainfall thresholds for early-warning purposes were to be selected.

Effective risk management in the area of the Gallivaggio sanctuary entailed assessing the location, magnitude, and time of any incipient failure that could not be contained by the existing protective barriers. Not only preserving public safety, but also avoiding unnecessary closures of the NR 36 was of fundamental importance to minimize socio-economic repercussions. Since damage accumulation prior to failure in a rock mass is frequently accompanied by measurable surface deformation (Sättele et al. 2016; Kromer et al. 2017), slope monitoring was deemed as the essential tool for pursuing these tasks. The GBInSAR ensured a wide and continuous coverage of the rock wall, and made it

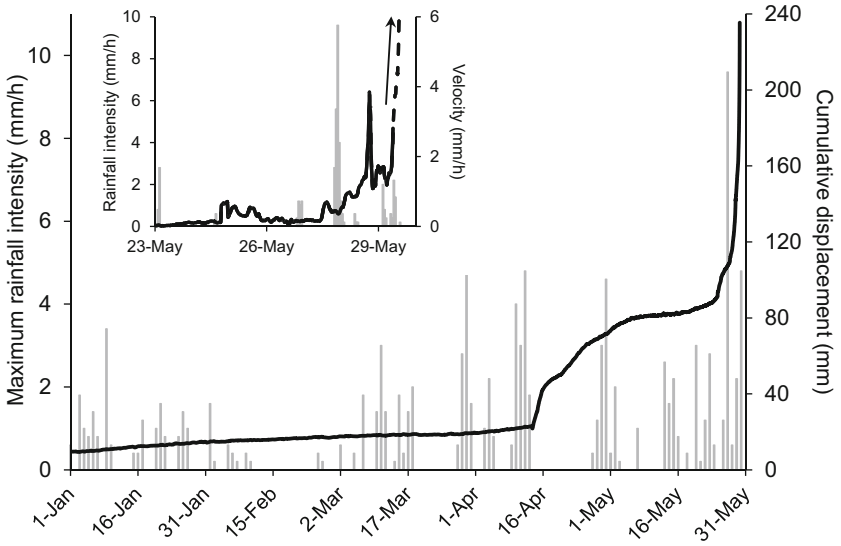

Fig. 12 Rainfall intensity versus displacement–velocity of the instability from January to May 2018. For illustrative purposes, displacement–velocity data correspond to the average of the ten control points in Fig. 6

possible to evaluate in detail the whole evolution of the ~ 5000 m^3 instability by coupling time series and interferogram data.

The integration of GBInSAR monitoring with a sequence of alert thresholds gave authorities an objective criterion of decision making for the issuing of restrictive orders prior to the 29 May 2018 failure. In light of the prompt identification of the tertiary creep stage, a precise failure-time prediction was obtained with appropriate notice by means of the inverse velocity method. Similarly, Hao's method (Hao et al. 2016, 2017) was applied for the first time to predict the failure of a natural slope, although plot convergence was only observed closer to the event. Thanks to the timely evacuation of the area, no injuries or fatalities were counted.

All these considerations rely on the assumption that rock slopes are characterized by detectable signs of progressive failure. In practice, rockfall scale can be a substantial hindrance to the ability of GBInSAR of capturing precursors; the unforeseen minor rockfalls (volume of few m^3) on 7 June 2017 and 13 April 2018 exemplify this drawback. First, minor rockfalls may imply very rapid processes of failure development and thus not exhibit clear precursors. Secondly, data quality may crucially degrade if the surface of the deforming slope sector makes up for only a fraction of a single pixel. In that case, displacement measurements may be skewed by the surrounding stable sectors and by processing artifacts. If possible, monitoring and early warning should be combined with active and/or passive defense systems as project demands allow. These should at least be designed to take into account failure volumes potentially invisible to the spatial resolution of the instrument. Further drawbacks of GBInSAR include its significant cost and the need for knowing the general area of instability prior to setting up the device. Moreover, a continuous power source and remote connectivity are indispensable to the successful implementation of the early-warning system. For these reasons, GBInSAR monitoring may be prohibitive for applications on a wider scale with respect to the conditions herein described, in remote regions, and in otherwise challenging contexts, for which external triggering monitoring might be preferable.

In general, the case study provides a reference framework for monitoring instabilities and managing associated risks in areas critically exposed to rockfalls and related slope hazards. Detecting ongoing progressive failures and estimating failure volumes will allow reducing uncertainties in the quantification of risk and in the definition of mitigation strategies. This will ultimately support the delineation of emergency protocols and the communication of evacuation orders.

Acknowledgements

This work has been sponsored by the Italian National Civil Protection Department (DPC) and by the Regional Agency for Environmental Protection of the Lombardia Region (ARPA-Lombardia). The Center for Geological Monitoring of ARPA-Lombardia conducted the surveillance activity and ground checks on site and managed the operations control room during phases of emergency. DPC and ARPA-Lombardia are acknowledged for supporting the project and for giving the permission for publication. The GBInSAR system used in this application was designed and produced by Ellegi LLC, a European Commission Joint Research Centre spin-off, using proprietary GBInSAR LiSALab technology.

References

Atzeni C, Barla M, Pieraccini M, Antolini F (2015) Early warning monitoring of natural and engineered slopes with ground-based synthetic-aperture radar. Rock Mech Rock Eng 48(1):235–246

Barla G, Antolini F, Barla M, Mensi E, Piovano G (2010) Monitoring of the Beauregard landslide (Aosta Valley, Italy) using advanced and conventional techniques. Eng Geol 116(3–4):218–235
Barla M, Antolini F, Bertolo D, Thuegaz P, D'Aria D, Amoroso G (2017) Remote monitoring of the Comba Citrin landslide using discontinuous GBInSAR campaigns. Eng Geol 222:111–123
Baudin T, Maruqer D, Persoz F (1993) Basement-cover relationships in the Tambo nappe (Central Alps, Switzerland): geometry, structure and kinematics. J Struct Geol 15(3–5):543–553
Carlà T, Farina P, Intrieri E, Botsialas K, Casagli N (2017) On the monitoring and early-warning of brittle slope failures in hard rock masses: examples from an open-pit mine. Eng Geol 228:71–81
Casagli N, Catani F, Del Ventisette C, Luzi G (2010) Monitoring, prediction, and early warning using ground-based radar interferometry. Landslides 7(3):291–301
Chau KT, Wong RHC, Liu J, Lee CF (2003) Rockfall hazard analysis for Hong Kong based on rockfall inventory. Rock Mech Rock Eng 36(5):383–408
Cornelius RR, Scott PA (1993) A materials failure relation of accelerating creep as empirical description of damage accumulation. Rock Mech Rock Eng 26(3):233–252
Cossart E, Braucher R, Fort M, Bourlès DL, Carcaillet J (2008) Slope instability in relation to glacial debuttressing in alpine areas (upper durance catchment, southeastern France): evidence from field data and ^{10}Be cosmic ray exposure ages. Geomorphology 95(1–2):3–26
Crosta GB, Agliardi F (2003) Failure forecast for large rock slides by surface displacement measurements. Can Geotech J 40(1):176–191
Del Ventisette C, Casagli N, Fortuny-Guasch J, Tarchi T (2012) Ruinon landslide (Valfurva, Italy) activity in relation to rainfall by means of GBInSAR monitoring. Landslides 9(4):497–509
Eberhardt E, Stead D, Stimpson B, Read RS (1998) Identifying crack initiation and propagation thresholds in brittle rock. Can Geotech J 35(2):222–233
Farina P, Coli N, Yön R, Eken G, Ketizmen H (2013) Efficient real time stability monitoring of mine walls: the Çöllolar mine case study. Proceedings, 23rd International Mining Congress & Exhibition of Turkey. Antalya:111–117
Federico A, Popescu M, Elia G, Fidelibus C, Internò G, Murianni A (2012) Prediction of time to slope failure: a general framework. Environ Earth Sci 66(1):245–256
Ferrari F, Apuani T, Giani GP (2014) Rock mass rating spatial estimation by geostatistical analysis. Int J Rock Mech Min Sci 70:162–176
Fukuzono T (1985) A new method for predicting the failure time of a slope. Proceedings, 4th international conference and field workshop in landslides, Tokyo, pp 145–150
Hao S, Liu C, Lu C, Elsworth D (2016) A relation to predict the failure of materials and potential application to volcanic eruptions and landslides. Sci Rep 6:27877
Hao S, Yang H, Elsworth D (2017) An accelerating precursor to predict "time-to-failure" in creep and volcanic eruptions. J Volcanol Geotherm Res 343:252–262
Hungr O, Evans SG, Hazzard J (1999) Magnitude and frequency of rock falls and rock slides along the main transportation corridors of southwestern British Columbia. Can Geotech J 36(2):224–238
Hungr O, Leroueil S, Picarelli L (2014) The Varnes classification of landslide types, an update. Landslides 11(2):167–194
Intrieri E, Gigli G, Mugnai F, Fanti R, Casagli N (2012) Design and implementation of a landslide early warning system. Eng Geol 147–148:124–136
Kieffer DS, Valentin G, Unterberger K (2016) Continuous real-time slope monitoring of the Ingelsberg in bad Hofgastein, Austria. Geomech Tunnelling 9(1):37–44
Kilburn C (2012) Precursory deformation and fracture before brittle rock failure and potential application to volcanic unrest. J Geophys Res Solid Earth 117:B02211
Krautblatter M, Moser M (2009) A nonlinear model coupling rockfall and rainfall intensity based on a four year measurement in a high Alpine rock wall (Reintal, German Alps). Nat Hazards Earth Syst Sci 9:1425–1432
Kromer R, Lato M, Hutchinson DJ, Gauthier D, Edwards T (2017) Managing rockfall risk through baseline monitoring of precursors using a terrestrial laser scanner. Can Geotech J 54:953–967
Lato M, Hutchinson J, Diederichs M, Ball D, Harrap R (2009) Engineering monitoring of rockfall hazards along transportation corridors using mobile terrestrial LiDAR. Nat Hazards Earth Syst Sci 9:935–946
Lato MJ, Gauthier D, Hutchinson DJ (2015) Rock slopes asset management: selecting the optimal three-dimensional remote sensing technology. Transp Res Rec 2510:7–14
Leva D, Nico G, Tarchi D, Fortuny-Guasch J, Sieber AJ (2003) Temporal analysis of a landslide by means of a ground-based SAR interferometer. IEEE Trans Geosci Remote Sens 41(4):745–752
Loew S, Gschwind S, Gischig V, Keller-Signer A, Valenti G (2017) Monitoring and early warning of the 2012 Preonzo catastrophic rockslope failure. Landslides 14(1):141–154
Luzi G, Pieraccini M, Mecatti D, Noferini L, Macaluso G, Galgaro A, Atzeni C (2006) Advances in ground-based microwave interferometry for landslide survey: a case study. Int J Remote Sens 27(12):2331–2350
Macciotta R, Martin CD, Cruden DM (2015) Probabilistic estimation of rockfall height and kinetic energy based on a three-dimensional trajectory model and Monte Carlo simulation. Landslides 12(4):757–772
Macciotta R, Martin CD, Morgenstern NR, Cruden DM (2016) Quantitative risk assessment of slope hazards along a section of railway in the Canadian cordillera—a methodology considering the uncertainty in the results. Landslides 13(1):115–127
Marquer D, Baudin T, Peucat J-J, Persoz F (1994) Rb-Sr mica ages in the Alpine shear zones of the Truzzo granite: timing of the Tertiary alpine P-T-deformations in the Tambo nappe (Central Alps, Switzerland). Eclogae Geol Helv 87(1):225–239
Mateos RM, García-Moreno I, Azañón JM (2012) Freeze–thaw cycles and rainfall as triggering factors of mass movements in a warm Mediterranean region: the case of the Tramuntana Range (Majorca, Spain). Landslides 9(3):417–432
Mazzanti P, Bozzano F, Cipriani I, Prestininzi A (2015) New insights into the temporal prediction of landslides by a terrestrial SAR interferometry monitoring case study. Landslides 12(1):55–68
Mononen S, Suikkanen M, Coli N, Meloni F (2018) Use of radar system for real-time safety-critical slope monitoring at Yara Siilinjärvi mine, Finland. Proceedings, 2018 International Symposium on Slope Stability in Open Pit Mining and Civil Engineering, Seville
Monserrat O, Crosetto M, Luzi G (2014) A review of ground-based SAR interferometry for deformation measurement. ISPRS J Photogramm 93:40–48
Noferini L, Pieraccini M, Mecatti D, Macaluso G, Atzeni C, Mantovani M, Marcato G, Pasuto A, Silvano S, Tagliavini F (2007) Using GB-SAR technique to monitor slow moving landslide. Eng Geol 95(3–4):88–98
Petley DN, Bulmer MH, Murphy W (2002) Patterns of movement in rotational and translational landslides. Geology 30(8):719–722
Rose ND, Hungr O (2007) Forecasting potential rock slope failure in open pit mines using the inverse-velocity method. Int J Rock Mech Min Sci 44(2):308–320
Rosser N, Lim M, Petley D, Dunning S, Allison R (2007) Patterns of precursory rockfall prior to slope failure. J Geophys Res Earth Surf 112:F04014
Royán MJ, Abellán A, Vilaplana JM (2015) Progressive failure leading to the 3 December 2013 rockfall at Puigcercós scarp (Catalonia, Spain). Landslides 12(3):585–595
Salvini R, Francioni M, Riccucci S, Bonciani F, Callegari I (2013) Photogrammetry and laser scanning for analyzing slope stability and rock fall runout along the Domodossola–Iselle railway, the Italian Alps. Geomorphology 185:110–122
Sättele M, Krautblatter M, Bründl M, Straub D (2016) Forecasting rock slope failure: how reliable and effective are warning systems? Landslides 13(4):737–750
Schmid S, Rück P, Schreurs G (1990) The significance of the Schams Nappes for the paleotectonic and orogenic evolution of the Penninic Zone along the NFP 20 East traverse (Grisons, Eastern Switzerland). Mém Soc Géol Fr 156:263–287
Stock GM, Martel SJ, Collins BD, Harp EL (2012) Progressive failure of sheeted rock slopes: the 2009-2010 Rhombus Wall rock falls in Yosemite Valley, California, USA. Earth Surf Process Landf 37:546–561
Voight B (1989) A relation to describe rate-dependent material failure. Science 243(4888):200–203

T. Carlà (✉) · T. Nolesini · L. Solari · N. Casagli
Department of Earth Sciences,
University of Florence,
Via La Pira 4, 50121, Florence, Italy
Email: tommaso.carla@unifi.it

C. Rivolta
Ellegi srl,
Corso Magenta 12, 20123, Milan, Italy

L. Dei Cas
ARPA-Lombardia,
Center for Geological Monitoring,
Via del Gesù 17, 23100, Sondrio, Italy